AIAA JOURNAL
Vol. 35, No. 10, October 1997

Flow Model for Predicting Normal Shock Wave Induced Vortex Breakdown

M. K. Smart*
NASA Langley Research Center, Hampton, Virginia 23681
and
I. M. Kalkhoran†
Polytechnic University, Brooklyn, New York 11201

An analytical study of normal shock wave induced vortex breakdown has been undertaken. In this inviscid axisymmetric analysis, the response of supersonic streamwise vortices to imposed normal shocks has been determined by modeling the rotational core of the vortex as a slender, swirling layer. For vortex/shock combinations of increasing strength, the analysis predicts an ever increasing axial velocity deficit in the vortex core. Vortex breakdown is presumed to occur if a vortex/shock combination leads to flow stagnation at the vortex axis. The results of this study indicate that an inverse relationship exists between vortex swirl and freestream Mach number at breakdown. The breakdown limit curve generated using this analysis shows good correlation with established experimental results, indicating that the onset of normal shock wave induced vortex breakdown can be predicted with a relatively simple flow model and without recourse to numerical simulation. Interpretation of some normal shock wave/vortex interaction experiments in light of the predictions suggests that the phenomenon previously known as supersonic vortex distortion is a form of vortex breakdown.

Nomenclature

a	= speed of sound
c	= factor relating the swirl velocity before and after the shock
D	= $0.5(\gamma - 1)/a_t^2$
k	= $[2 + (\gamma - 1)M_1^2]/(\gamma + 1)/M_1^2$
M	= Mach number
P	= pressure
R	= vortex core radius
r	= radius
S	= vortex swirl parameter, Γ/RU_∞
U	= axial velocity
u, v, w	= velocity components
V	= $\sqrt{(u^2 + v^2)}$
x, y, z	= Cartesian coordinates
α	= vortex generator angle of attack
Γ	= circulation
ϵ	= $\Lambda_3^2 = \Lambda_1^2 c^2$
Λ	= swirl velocity at the edge of the vortex core
λ	= $U_3^2 - U_{3_0}^2 + \epsilon$
ρ	= density
τ	= vortex swirl ratio, Λ/U
ω_0	= $(P_{t_0} - P_0)/P_{t_0}$

Subscripts

ax	= axial component
R	= condition at the edge of the vortex core
sw	= swirl component
t	= stagnation conditions
0	= condition at the vortex axis
1	= station upstream of the shock
2	= station just downstream of the shock
3	= station a moderate distance downstream of the shock
∞	= freestream

Received March 8, 1997; revision received July 7, 1997; accepted for publication July 8, 1997.

*National Research Council Research Associate, Hypersonic Airbreathing Propulsion Branch, Mail Stop 168. Member AIAA.
†Associate Professor, Department of Mechanical, Aerospace, and Manufacturing Engineering. Senior Member AIAA.

Introduction

A CHARACTERISTIC of vortex cores with axes roughly parallel to a surrounding flow is the tendency for abrupt bursting or breakdown in the presence of certain decelerating influences. Studies of the flowfields generated by these encounters have been reported by many investigators since the late 1950s, including Lambourne and Bryer,[1] Harvey,[2] Faler and Leibovich,[3] Sarpkaya,[4] and Delery et al.,[5] to name a few. This phenomenon, which has become known as vortex breakdown, is generally characterized by a sudden increase in the size of the vortex core, appearance of stagnation point(s) on the vortex axis, a reversed flow region, and the presence of large-scale unsteadiness. It is an important flow feature in such diverse areas as low-speed combustion and the stability of high-speed aircraft.

As the body of knowledge concerning vortex breakdown has grown, it has become apparent that the phenomenon can take on many different forms. The major factors that influence vortex breakdown may be separated into the following four groups: 1) the velocity distribution in the vortex upstream of breakdown, 2) the strength and geometry of the decelerating influence, which generally takes the form of an externally imposed adverse pressure field, 3) Reynolds number effects, and 4) compressibility effects.

Theoretical treatments of vortex breakdown have dealt almost exclusively with incompressible flows up to the present day. Whereas compressibility effects have been known to be important, particularly in high-speed flows, the added complexity of dealing with compressibility has stifled production of useful results from theoretical analyses that include its effects. The focus of the current work is to develop a simplified physical model for the interaction between a normal shock and a streamwise vortex, a flow in which compressibility effects are paramount. This flow problem, known in the literature simply as normal shock wave/vortex interaction (NSVI), has recently been examined using both experiment and numerical simulation. However, detailed theoretical analyses are scarce.

The most comprehensive study of NSVI up to the present was performed by Delery et al.,[5] who examined the interaction between uniform axial velocity vortices and normal shocks generated by a pitot type inlet. In this combined experimental/numerical study, laser Doppler velocimetry and multihole conical probe measurements were reported before and after the shock, indicating that NSVI involving vortices above a certain strength led to vortex breakdown characterized by reverse flow on the vortex axis, reduction in the maximum swirl, and an increase in the radius of the vortex core.

A vortex breakdown limit was developed using the results of these experiments, indicating an inverse relationship between vortex swirl and shock strength at breakdown. The companion numerical study, which solved the axisymmetric Euler equations, produced a similar breakdown limit to the experiments, indicating that the onset of vortex breakdown is dominated by inviscid considerations in this instance. In contrast to the success in predicting the breakdown limit, these Euler simulations were not able to accurately calculate the observed flow structure after breakdown.

The interaction of normal shock waves with wakelike supersonic vortices generated by a swirling vane injector was studied experimentally by Metwally et al.[6] and Cattafesta and Settles.[7] Both studies reported a strong influence of vortex swirl and Mach number on the interaction, a vortex breakdown, and an oscillating bulged forward shock. The interaction of wakelike supersonic wing tip vortices with normal shock waves generated in front of a pitot type inlet was experimentally investigated by Kalkhoran et al.[8] These experiments indicated that NSVI involving moderate strength vortices leads to the formation of an unsteady conical shock wave far upstream of the inlet, which contains a conical flow with two distinct zones. This flow structure was noted to be identical to the vortex distortion observed in the head-on interaction of supersonic wing tip vortices with wedge leading edges reported by Kalkhoran.[9]

Numerical simulation of the NSVI problem is not extensive, partly due to the difficulty of calculating the unsteady breakdown flowfield. Apart from the Euler simulations of Ref. 5 already mentioned, Ref. 6 reported axisymmetric Navier–Stokes simulations, which generated a similar structure to that instantaneously observed to occur in the more severe experiments. These calculations predicted a stagnation point on the vortex axis and, therefore, were characterized as depicting a vortex breakdown. In addition, a recent study by Erlebacher et al.,[10] using the time-dependent Euler equations, reported a breakdown structure that exhibited substantial upstream influence.

The current investigation involves an analytical study of NSVI using a relatively simple flow model. This flow model is used to calculate the response of a streamwise vortex to an imposed normal shock and, further, to predict the onset of vortex breakdown in NSVI. It has been attempted to simplify the model as much as possible while retaining the physical mechanisms that are expected to dominate the prebreakdown shock/vortex interaction flowfield. The breakdown limit predicted using the analysis is compared with both experimental data and numerical simulation.

Theoretical Explanations of Vortex Breakdown

A number of different theories concerning the physical nature of vortex breakdown have been proposed over the years, the most prominent of which are described in review articles on the subject by Hall,[11] Leibovich,[12] and Delery.[13] The overwhelming majority of these theories fall into one of the following three categories, the basic ideas of which were described in Hall[11] as follows.

1) The phenomenon is analogous to the separation of a boundary layer.

2) The phenomenon is a consequence of hydrodynamic instability.

3) The phenomenon depends on the existence of a critical state.

Interestingly, predictions tabulated in Delery[13] from all three categories supply a similar critical value for the vortex swirl parameter, $S = \Gamma / RU_\infty$ above which an incompressible streamwise vortex with typical axial and swirling velocity profiles cannot exist. In the context of a streamwise vortex that encounters an adverse pressure field, breakdown is then predicted by these theories when the vortex swirl parameter locally reaches the critical value. Note that, although the overwhelming majority of these theories supply predictions for the onset of vortex breakdown, they do not enable calculation of the postbreakdown flowfield. Furthermore, almost all of these theoretical works have been restricted to an incompressible fluid and are not necessarily applicable to high-speed flows, particularly when shock waves are present.

The NSVI analysis presented in the current article is based on the idea listed as category 1, i.e., that the occurrence of vortex breakdown is a dynamic phenomenon similar to the separation of a boundary layer. The physical reasoning behind this idea was described in Ref. 11. It is based on the fact that vortices are regions of low total pressure relative to the surrounding flow and, hence, are more easily brought to rest by an applied pressure gradient. To elucidate the particular process by which this occurs in an incompressible vortex, the quasicylindrical equations were used in Ref. 11 to show that an externally applied axial pressure gradient is magnified at the vortex axis. This magnification of externally applied pressure fields, which is peculiar to vortices, was considered by Hall[11] to be the driving force toward flow stagnation on the vortex axis and the subsequent breakdown of the vortex structure. The NSVI flowfield is examined in the current work to see if these same physical mechanisms apply when a normal shock wave is imposed on the vortex.

Flow Model for Predicting Normal Shock Wave Induced Vortex Breakdown

The aim of the following analysis is to determine the streamwise vortex strength above which the imposition of a normal shock wave leads to vortex breakdown. As the presence of a stagnation point on the axis of a streamwise vortex is one of the major characterizing features of vortex breakdown, the predicted presence of zero axial velocity at the vortex axis is considered to be an indicator of vortex breakdown. To achieve the aforementioned aim, established knowledge concerning the response of streamwise vortices to imposed shock waves has been utilized. This has enabled the development of a relatively simple flow model for predicting normal shock wave induced vortex breakdown.

Streamwise vortices generally result from the separation and subsequent rollup of boundary layers. Any number of geometrical configurations may generate streamwise vortices in high Reynolds number flows; however, a moderate distance downstream of separation most streamwise vortices develop into a slender swirling flow with minimal streamwise development and nearly axisymmetric shape. In a typical streamwise vortex, the radial velocity is small; the axial velocity may be wakelike, uniform, or jetlike (depending on the method of generation); and the swirl velocity is similar to that of a Burgers' vortex. The universality of the fully developed form exhibited by almost all streamwise vortices suggests that this form is a stable solution of the Navier–Stokes equations for a region of concentrated vorticity convecting within a relatively uniform flow at high Reynolds number. A number of analytical studies have also indicated this fact.[14, 15] In the remainder of the article, this form will be referred to as that pertaining to a fully developed vortex.

Now consider the case where a fully developed streamwise vortex encounters an externally imposed normal shock. Given the aforementioned stability of the fully developed vortex form, it is reasonable to expect that a moderate distance downstream of the shock, the vortex will return to this form as long as it does not undergo a catastrophic flow reorganization such as vortex breakdown. Experimental work may be cited as evidence of this tendency of perturbed vortices to return to fully developed form. In the experiments reported in Ref. 5, it was observed that in the absence of vortex breakdown, "the general structure of the vortex undergoes no basic change when passing through the shock." In particular, the downstream flow was found to retain a regular shape, with the swirl velocity distribution remaining practically invariant, but with the axial velocity component at the vortex axis dropping below the freestream value to form a wakelike profile. The results presented in Ref. 5 clearly showed that, in the absence of vortex breakdown, vortices reform in the manner suggested even after the abrupt disruption of an imposed normal shock.

In light of these ideas, a flow model for the response of a supersonic streamwise vortex to an imposed normal shock that does not cause vortex breakdown is presented in Fig. 1. Consider a fully developed streamwise vortex with typical axisymmetric velocity profiles being convected within a surrounding uniform stream. At some streamwise station, a normal shock is imposed on the vortex. Because of the entropy variations inherent in the vortex, the shock cannot remain normal in the viscous core and must curve forward, as shown in Fig. 1. It will, however, return to being normal to the flow at the vortex axis to maintain symmetry. A moderate distance downstream of the shock the vortex will have an increased core size, a reduced swirl magnitude to conserve angular momentum, and an axial velocity profile that is more wakelike than before the disturbance. In addition to these characteristics, it is assumed that the

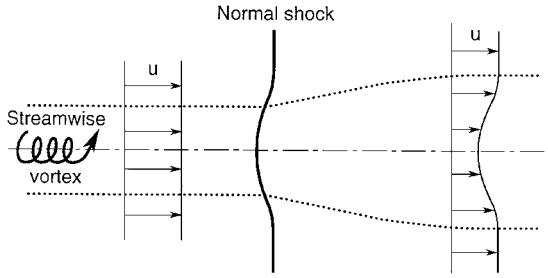

Fig. 1 Flowfield model for NSVI that does not lead to breakdown.

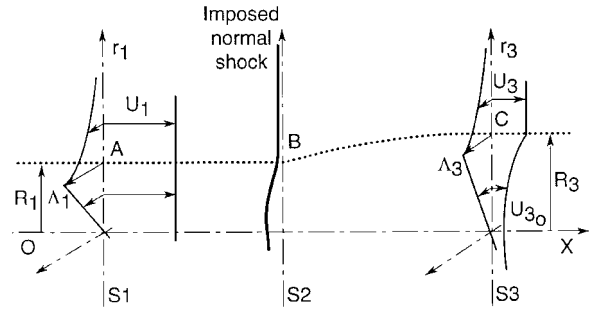

Fig. 2 Schematic of the flow model used for the NSVI analysis.

swirl distribution of the disturbed vortex returns to fully developed. Along with the choice of a sensible profile for the postdisturbance axial velocity, this assumption enables closure of the downstream flow properties by straightforward integration of the conservation equations across the vortex core.

The flow model of Fig. 1 can be used to determine the effect of imposed shocks on a given streamwise vortex. Alternatively, the model can be used to assess the response of different vortices to a given shock wave. In a manner similar to results reported in Ref. 5, the current flow model indicates that an increase in the magnitude of the imposed pressure rise or vortex circulation leads to an ever increasing axial velocity deficit downstream of the shock. Furthermore, for certain combinations of strong vortices and/or intense shocks, the flow model predicts stagnation of the flow at the vortex axis. As a stagnation point is one of the defining characteristics of vortex breakdown, its prediction by the current flow model for a particular vortex/shock combination is interpreted to be an indication that the vortex/shock combination leads to vortex breakdown.

The physical mechanism that leads to vortex breakdown in this instance is quite straightforward. Just behind the shock, the vortex structure is determined by its upstream properties and the shock shape, i.e., its structure can be quite different from a fully developed form. It responds to this situation by relaxing toward a fully developed vortex form that matches its new external conditions. In some cases the imposed change is so great (or the vortex is so strong) that, in the process of adapting to the new external conditions, the inner portion of the vortex core (which can be a region of very low total pressure) is stagnated. Once the vortex stagnates at its axis, its entire structure becomes unstable, and it then suffers a major reorganization or breakdown.

Breakdown Limit for NSVI

A breakdown limit curve for supersonic streamwise vortices in the presence of externally applied normal shocks is developed in this section. This limit is generally applicable to a free vortex, i.e., a vortex that is not confined in the radial direction. In the analysis, the working fluid is assumed to be a perfect gas with constant ratio of specific heats γ; the vortex core and the surrounding stream are assumed to have a uniform stagnation enthalpy; and stagnation pressure is assumed to remain constant along each streamline, except when crossing the shock. For simplicity of presentation, the analysis is applied using the Rankine vortex as an approximation to the fully developed vortex form; however, the method can be implemented using more realistic vortex models. Inherent in the use of a Rankine vortex model is the assumption that the radius of the vortex core is the dominant scaling parameter in the flow.

As the vast majority of flows where compressibility is important also have high Reynolds number, some assumptions applicable to flows with high Reynolds number are utilized. In particular, the analysis shares some characteristics with integral methods commonly used for boundary layers. First, the effect of vortex core growth on the irrotational outer flow is neglected in the same way that boundary-layer growth is assumed to not affect the surface pressure distribution in a boundary-layer calculation. This approximation is considered reasonable within the constraints of the analysis, i.e., in the absence of flow stagnation or vortex breakdown, when flow outside the vortex core is known to remain relatively unaffected by changes in the core region.[5] Second, to integrate across the vortex core, a postdisturbance axial velocity profile is chosen in advance in the same way that a velocity profile is specified a priori in integral boundary-layer methods.

Figure 2 shows an annotated schematic of the flow model used for the analysis. S1, S2, and S3 represent three stations along an axisymmetric vortex with axis OX. Flow between S1 and S3 is assumed to be inviscid, steady, and compressible, and line ABC indicates the edge of the vortex core outside of which the flow is assumed to be irrotational. The prescribed vortex velocity distributions at S1 are as follows.

1) Axial velocity $u_1 = \text{const} = U_1$ for all r_1.

2) Swirl velocity v_1 is given by

$$v_1 = \Lambda_1 R_1 / r_1 \qquad (r_1 \geq R_1)$$

$$v_1 = \Lambda_1 r_1 / R_1 \qquad (r_1 \leq R_1)$$

3) Radial velocity $w_1 = 0$.

For an axisymmetric compressible vortex with the mentioned velocity components, the radial momentum equation reduces to

$$\frac{v_1^2}{r_1} = \frac{1}{\rho}\frac{\partial P_1}{\partial r_1} \tag{1}$$

To integrate Eq. (1) to obtain the pressure distribution at S1, a relationship between the density and the pressure is needed. The energy equation for a perfect gas supplies the following expression for density in terms of pressure, velocity, and other parameters that are constant throughout the flow:

$$\rho = \frac{\gamma P / a_t^2}{1 - DV^2} \tag{2}$$

Substituting Eq. (2) into Eq. (1) yields

$$\frac{v_1^2}{r_1} = \frac{1 - DV^2}{\gamma P_1 / a_t^2}\frac{\partial P_1}{\partial r_1} \tag{3}$$

Integration of Eq. (3) from the edge of the core ($r_1/R_1 = 1$) to the outer streamline ($r_1/R_1 \longrightarrow \infty$) using $V^2 = U_1^2 + \Lambda_1^2(R_1/r_1)^2$ yields

$$\left(\frac{P_{1_R}}{P_{1_\infty}}\right)^{(\gamma-1)/\gamma} = \frac{1 - D(U_1^2 + \Lambda_1^2)}{1 - DU_1^2} \tag{4}$$

Integration of Eq. (3) from a point inside the core to the edge of the core using $V^2 = U_1^2 + \Lambda_1^2(r_1/R_1)^2$ yields the pressure distribution inside the vortex core at S1 as follows:

$$\left(\frac{P_1}{P_{1_\infty}}\right)^{(\gamma-1)/\gamma} = \frac{\left[1 - D(U_1^2 + \Lambda_1^2)\right]^2}{(1 - DU_1^2)\left\{1 - D\left[U_1^2 + \Lambda_1^2(r_1/R_1)^2\right]\right\}} \qquad (r_1 \leq R_1) \tag{5}$$

Substitution of Eq. (2) into Eq. (5) yields the density distribution inside the vortex core at S1 to be

$$\frac{\rho_1}{\rho_{1_\infty}} = \frac{\left[1 - D(U_1^2 + \Lambda_1^2)\right]^{2\gamma/(\gamma-1)}}{\left\{1 - D\left[U_1^2 + \Lambda_1^2(r_1/R_1)^2\right]\right\}^{(2\gamma-1)/(\gamma-1)}(1 - DU_1^2)^{1/(\gamma-1)}} \qquad (r_1 \leq R_1) \tag{6}$$

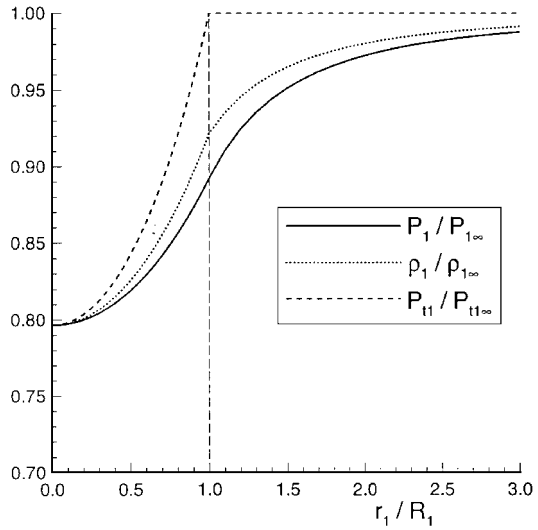

Fig. 3 Pressure, density, and stagnation pressure distributions at S1 for a streamwise vortex with $U_1 = 600$ m/s, $M_1 = 2.0$, and $\Lambda_1 = 120$ m/s in air.

Similarly, the distribution of stagnation pressure inside the vortex core at S1 is given by

$$\left(\frac{P_{t1}}{P_{t1_\infty}}\right)^{(\gamma-1)/\gamma} = \frac{\left[1 - D(U_1^2 + \Lambda_1^2)\right]^2}{(1 - DU_1^2)\left\{1 - D\left[U_1^2 + \Lambda_1^2(r_1/R_1)^2\right]\right\}^2} \qquad (r_1 \leq R_1) \quad (7)$$

Typical radial distributions of pressure, density, and stagnation pressure for a streamwise compressible vortex used in the analysis are shown in Fig. 3.

A normal shock is now imposed on the vortex at S2 (see Fig. 2). To determine the effect of this imposed disturbance, it is assumed that at a station S3, a moderate distance downstream of S2, the vortex has returned to Rankine form but with variable axial velocity. To ascertain the character of the vortex at S3 in this instance, the following assumptions are made concerning the irrotational outer flow.

1) The imposed pressure rise is applied as a boundary condition at $r \to \infty$; hence,

$$P_3(r \to \infty) = P_{3_\infty} = P_{1_\infty} + \Delta P_{\text{shock}}$$

2) The axial velocity outside the vortex core is constant; hence,

$$u_3 = U_3 \qquad (r_3 \geq R_3)$$

3) The swirl velocity is of irrotational form, differing in magnitude from the swirl at S1 by an unknown factor c. Therefore,

$$v_3 = \Lambda_1 c R_3 / r_3 \qquad (r_3 \geq R_3)$$

4) Radial velocity $w_3 = 0$.

These assumptions may be interpreted as neglecting the feedback effect of the perturbed vortex core on the outer flow. In other words, as far as the response of the vortex core is concerned, the form of the outer flow is unaffected by changes in the vortex core behind the shock. Having defined the outer flow at S3, the following assumptions are made concerning flow inside the vortex core at S3.

1) The radius of the vortex core changes to R_3.

2) The axial velocity distribution inside the vortex core takes the form

$$u_3 = \sqrt{U_{3_0}^2 + (U_3^2 - U_{3_0}^2)(r_3/R_3)^2} \qquad (r_3 \leq R_3)$$

This profile is smoothly varying inside the vortex core, has zero slope at the vortex axis, and matches the outer flow at the edge of the core. Whereas use of this velocity profile constitutes an approximation to the real flow properties at S3, it does represent a shape that is consistent with the velocity measurements reported in Ref. 5.

3) The swirl velocity has a Rankine vortex form that matches the outer flow at the edge of the core

$$v_3 = \Lambda_1 c r_3 / R_3 \qquad (r_3 \leq R_3)$$

4) Radial velocity $w_3 = 0$.

Given the aforementioned velocity distributions at S3, integration of the radial momentum equation in a fashion similar to that performed at S1 yields the pressure distribution inside the vortex core at S3 as follows:

$$\left(\frac{P_3}{P_{3_\infty}}\right)^{(\gamma-1)/\gamma} = \left\{\frac{1 - D(U_3^2 + \epsilon)}{1 - D\left[U_{3_0}^2 + \lambda(r_3/R_3)^2\right]}\right\}^{\epsilon/\lambda} \frac{1 - D(U_3^2 + \epsilon)}{1 - DU_3^2} \qquad (r_3 \leq R_3) \quad (8)$$

The corresponding density distribution inside the vortex core at S3 is, therefore,

$$\frac{\rho_3}{\rho_{3_\infty}} = \frac{\left[1 - D(U_3^2 + \epsilon)\right]^{\{1 + [(\lambda + \gamma\epsilon)/(\gamma-1)\lambda]\}}}{\left\{1 - D\left[U_{3_0}^2 + \lambda(r_3/R_3)^2\right]\right\}^{\{1 + [\gamma\epsilon/(\gamma-1)\lambda]\}} (1 - DU_3^2)^{1/(\gamma-1)}} \qquad (r_3 \leq R_3) \quad (9)$$

The stagnation pressure distribution at S3 will be dependent on both the stagnation pressure distribution at S1 and the shock wave shape and is, therefore, difficult to determine. However, the stagnation pressure on the vortex axis can be calculated using the normal shock relations, as the shock wave must be normal to the flow at the vortex axis.

The listed assumptions imply that, downstream of the shock, the vortex returns to a fully developed form with an axial velocity profile that may vary across the vortex core. As already noted, streamwise vortices are more easily decelerated by a flow retardation than the surrounding flow. The assumed u_3 profile in the vortex core allows the core to develop a wakelike profile at S3 in response to the imposed pressure rise. It must be clearly stated, however, that flow properties at S3 are not assumed a priori to have a wakelike axial velocity, an enlarged core, or a reduced swirl. Whether each of these characteristics of the flowfield increases or decreases between S1 and S3 is determined by solution of the conservation equations.

Now that the form of the vortical flow at S3 has been established, the vortex core flow at S1 and S3 can be related by the conservation equations to determine the unknowns at S3, namely, U_{3_0}, R_3, and c. The three equations used to solve for the unknowns are 1) conservation of mass flow in the vortex core between S1 and S3, 2) conservation of angular momentum flow in the vortex core between S1 and S3, and 3) Bernoulli's equation at the vortex axis between S1 and S3.

Conservation of Mass Flow in the Vortex Core

Equating the mass flow through stations S1 and S3 in the vortex core leads to the relation

$$\rho_{1_\infty} U_1 \int_0^{R_1} \frac{\rho_1}{\rho_{1_\infty}} r_1 \, dr_1 = \rho_{3_\infty} \int_0^{R_3} \frac{\rho_3}{\rho_{3_\infty}} u_3 r_3 \, dr_3$$

For a normal shock, $\rho_{2_\infty}/\rho_{1_\infty}$ is a function of M_1 as follows:

$$\frac{\rho_{2_\infty}}{\rho_{1_\infty}} = \frac{U_1}{U_2} = \frac{(\gamma+1)M_1^2}{2 + (\gamma-1)M_1^2} = \frac{1}{k} \qquad (10)$$

Properties on the outer streamline ($r_1/R_1 \to \infty$) do not change between S2 and S3; hence, $P_{3_\infty} = P_{2_\infty}$, $U_3 = U_2$, $P_{t3_\infty} = P_{t2_\infty}$, and $\rho_{3_\infty} = \rho_{2_\infty}$. Given this, conservation of core mass flow yields

$$k R_1^2 \int_0^1 \frac{\rho_1}{\rho_{1_\infty}} \frac{r_1}{R_1} \, d\left(\frac{r_1}{R_1}\right) = R_3^2 \int_0^1 \frac{\rho_3}{\rho_{3_\infty}} \frac{u_3}{U_1} \frac{r_3}{R_3} \, d\left(\frac{r_3}{R_3}\right) \qquad (11)$$

Substituting Eqs. (6) and (9) for the density distributions in Eq. (11) supplies the full equation for conservation of mass flow in the vortex core as follows:

$$\frac{k R_1^2 \left[1 - D(U_1^2 + \Lambda_1^2)\right]^{2\gamma/(\gamma-1)}}{(1 - DU_1^2)^{1/(\gamma-1)}} I_{m_1} = \frac{R_3^2 \left[1 - D(U_3^2 + \epsilon)\right]^{\{1 + [(\lambda + \gamma\epsilon)/(\gamma-1)\lambda]\}}}{(1 - DU_3^2)^{1/(\gamma-1)}} I_{m_3} \qquad (12)$$

where

$$I_{m_1} = \frac{\gamma - 1}{2\gamma D\Lambda_1^2}\left\{\left[1 - D(U_1^2 + \Lambda_1^2)\right]^{-\gamma/(\gamma-1)} - (1 - DU_1^2)^{-\gamma/(\gamma-1)}\right\}$$

and

$$I_{m_3} = \int_0^1 \frac{(u_3/U_1)(r_3/R_3)\,\mathrm{d}(r_3/R_3)}{\left\{1 - D\left[U_{3_0}^2 + \lambda(r_3/R_3)^2\right]\right\}^{\{1+[\gamma\epsilon/(\gamma-1)\lambda]\}}}$$

Conservation of Angular Momentum Flow in the Vortex Core

Equating the angular momentum flow through stations S1 and S3 in the vortex core leads to the relation

$$kR_1^3\int_0^1 \frac{\rho_1}{\rho_{\infty}}\left(\frac{r_1}{R_1}\right)^3 \mathrm{d}\left(\frac{r_1}{R_1}\right) = cR_3^3\int_0^1 \frac{\rho_3}{\rho_{\infty}}\frac{u_3}{U_1}\left(\frac{r_3}{R_3}\right)^3 \mathrm{d}\left(\frac{r_3}{R_3}\right) \tag{13}$$

Substituting Eqs. (6) and (9) for the density distributions in Eq. (13) supplies the full equation for conservation of angular momentum flow in the vortex core between S1 and S3 as follows:

$$\frac{kR_1^3\left[1 - D(U_1^2 + \Lambda_1^2)\right]^{2\gamma/(\gamma-1)}}{(1 - DU_1^2)^{1/(\gamma-1)}} I_{a_1} = \frac{cR_3^3\left[1 - D(U_3^2 + \epsilon)\right]^{\{1+[(\lambda+\gamma\epsilon)/(\gamma-1)\lambda]\}}}{(1 - DU_3^2)^{1/(\gamma-1)}} I_{a_3} \tag{14}$$

where

$$I_{a_1} = \frac{\gamma - 1}{2\gamma D^2\Lambda_1^4}(1 - DU_1^2)\left\{\left[1 - D(U_1^2 + \Lambda_1^2)\right]^{[-\gamma/(\gamma-1)]} - (1 - DU_1^2)^{[-\gamma/(\gamma-1)]}\right\} - \frac{\gamma - 1}{2D^2\Lambda_1^4} \times \left\{\left[1 - D(U_1^2 + \Lambda_1^2)\right]^{-[1/(\gamma-1)]} - (1 - DU_1^2)^{-[1/(\gamma-1)]}\right\}$$

and

$$I_{a_3} = \int_0^1 \frac{(u_3/U_1)(r_3/R_3)^3\,\mathrm{d}(r_3/R_3)}{\left\{1 - D\left[U_{3_0}^2 + \lambda(r_3/R_3)^2\right]\right\}^{\{1+[\gamma\epsilon/(\gamma-1)\lambda]\}}}$$

Bernoulli's Equation at the Vortex Axis

Bernoulli's equation cannot be applied across the shock wave; however, it can be used downstream of the shock to relate properties at S2 and S3. Application of the compressible Bernoulli's equation at the vortex axis between stations S2 and S3 yields

$$DU_2^2 + \left(\frac{P_{2_0}}{P_{2_\infty}}\right)^{(\gamma-1)/\gamma}\left(\frac{P_{2_\infty}}{P_{t2_0}}\right)^{(\gamma-1)/\gamma} = DU_3^2 + \left(\frac{P_{3_0}}{P_{3_\infty}}\right)^{(\gamma-1)/\gamma}\left(\frac{P_{3_\infty}}{P_{t3_0}}\right)^{(\gamma-1)/\gamma} \tag{15}$$

Given that the shock is normal at the vortex axis, we have

$$\frac{P_{2_\infty}}{P_{1_\infty}} = \frac{P_{2_0}}{P_{1_0}} = 1 + \frac{2\gamma}{\gamma+1}(M_1^2 - 1) = \Psi_p \tag{16a}$$

$$\frac{P_{t2_\infty}}{P_{t1_\infty}} = \frac{P_{t2_0}}{P_{t1_0}} = \left[\frac{(\gamma+1)M_1^2}{2 + (\gamma-1)M_1^2}\right]^{\gamma/(\gamma-1)} \times \left[\frac{\gamma+1}{2\gamma M_1^2 - (\gamma - 1)}\right]^{1/(\gamma-1)} = \Psi_t \tag{16b}$$

Use of Eqs. (10), (16a), and (16b) enables the left-hand side of Eq. (15) to be expressed in terms of prescribed properties as follows:

$$Dk^2U_1^2 + \left(\frac{P_{1_0}}{P_{1_\infty}}\right)^{(\gamma-1)/\gamma}\left(\frac{P_{1_\infty}}{P_{t1_0}}\right)^{(\gamma-1)/\gamma}\left(\frac{\Psi_p}{\Psi_t}\right)^{(\gamma-1)/\gamma} = DU_3^2 + \left(\frac{P_{3_0}}{P_{3_\infty}}\right)^{(\gamma-1)/\gamma}\left(\frac{P_{3_\infty}}{P_{t3_0}}\right)^{(\gamma-1)/\gamma} \tag{17}$$

The stagnation pressure does not change along streamlines between S2 and S3; hence,

$$(P_{3_\infty}/P_{t3_0}) = (P_{2_\infty}/P_{t2_0}) = (P_{1_\infty}/P_{t1_0})(\Psi_p/\Psi_t) \tag{18}$$

Using Eq. (18) and substituting Eqs. (5) and (8) for the pressure distributions, Bernoulli's equation leads to the following relation:

$$Dk U_1^2 + \frac{\left[1 - D(U_1^2 + \Lambda_1^2)\right]^2}{(1 - DU_1^2)^2}\left(\frac{P_{1_\infty}}{P_{t1_0}}\frac{\Psi_p}{\Psi_t}\right)^{(\gamma-1)/\gamma} = DU_{3_0}^2 + \left[\frac{1 - D(U_3^2 + \epsilon)}{1 - DU_{3_0}^2}\right]^{\epsilon/\lambda}\left[\frac{1 - D(U_3^2 + \epsilon)}{1 - DU_3^2}\right] \times \left(\frac{P_{1_\infty}}{P_{t1_0}}\frac{\Psi_p}{\Psi_t}\right)^{(\gamma-1)/\gamma} \tag{19}$$

Results and Discussion

Equations (12), (14), and (19) are three equations in the three unknowns R_3, c, and U_{3_0}. They form a set of simultaneous nonlinear algebraic equations and can be solved using a Newton–Raphson root finding technique for a given set of prescribed flow conditions. A Fortran computer program was written to perform this task. As is usual in the solution of sets of nonlinear algebraic equations, it was found that the choice of the initial estimate for the three unknowns was critical for a meaningful solution of the equation set to be found. In general, the use of initial estimates $R_3/R_1 = 1.0$, $U_{3_0} = U_3$, and $c = 1.0$ led to quick convergence.

This analysis can be used for two different tasks. First, it can be used to determine the state of a given supersonic streamwise vortex after the imposition of a shock that does not induce vortex breakdown. Second, it can be used to predict the vortex strength above which the imposition of a shock produces a stagnation point at the vortex axis, i.e., vortex breakdown. A typical result of use of the analysis for the first task is shown in Table 1. The first column of Table 1 shows the properties of a typical streamwise vortex in a Mach 2.0 airflow; the second column shows the predicted properties in the vortex well downstream of a normal shock ($P_{3_\infty}/P_{1_\infty} = 4.50$). The strength of the incoming vortex is characterized in the current work by the swirl ratio $\tau = \Lambda_1/U_1$, which for the example is $\tau = 0.20$. As expected, the flow responds to the shock with an expansion of the vortex core, a reduced swirl velocity, and development of a wakelike streamwise velocity profile.

It is interesting to examine the shock induced changes in the vortex in comparison to the case of an incompressible vortex in the presence of an adverse pressure gradient. Hall[11] attributed the breakdown of an incompressible vortex to vortical magnification of the imposed pressure rise. In the notation of the current work, a corresponding magnification would be indicated by a value of $(P_{3_0} - P_{1_0})/(P_{3_\infty} - P_{1_\infty}) > 1.0$. In the current example $(P_{3_0} - P_{1_0})/(P_{3_\infty} - P_{1_\infty}) = 0.924$, and so the pressure rise of the imposed shock is not magnified at the vortex axis. Although vortical pressure magnification does not occur, it is clear that the normal shock moves the vortex closer to breakdown, as indicated by the wakelike axial velocity after the shock. A useful parameter for gauging the closeness of a vortex to its breakdown limit is ω_0, the normalized difference between the stagnation and static pressure at the vortex axis, which approaches zero as the vortex stagnates. For the example listed in Table 1, $\omega_0 = 0.872$ in the undisturbed vortex and $\omega_0 = 0.285$ after the shock.

Table 1 Vortex properties before and after a shock that does not induce breakdown

Incoming vortex	Properties after imposed normal shock ($P_{3_\infty}/P_{1_\infty} = 4.50$)
$M_1 = 2.0$	$M_3 = 0.577$
$U_1 = 600$ m/s	$U_3 = 225.0$ m/s
$a_1 = 300$ m/s	$U_{3_0} = 157.3$ m/s
$\Lambda_1 = 120$ m/s	$R_3/R_1 = 1.045$
$\tau = \Lambda_1/U_1 = 0.20$	$\Lambda_3 = c\Lambda_1 = 109.4$ m/s
$P_{1_0}/P_{1_\infty} = 0.796$	$P_{3_0}/P_{3_\infty} = 0.896$
$\rho_{1_0}/\rho_{1_\infty} = 0.796$	$\rho_{3_0}/\rho_{3_\infty} = 0.866$

The significant reduction in ω_0 across the shock, in the absence of pressure magnification at the vortex axis, indicates that the physical mechanisms that lead to shock induced breakdown are different from those that occur when an incompressible vortex encounters an adverse pressure gradient.

The main interest of the current work is to use the analysis to determine a breakdown limit for NSVI. The onset of vortex breakdown in this case is signified by $U_{3_0} = 0$. Because the derived equations must be solved as a set, the best way to determine the vortex breakdown limit for a given external flow is to increase the swirl ratio gradually over a number of runs until $U_{3_0}/U_1 = 0$. For example, having chosen the incoming freestream properties and normal shock strength (γ, U_1, and M_1), the analysis can be performed for a very weak vortex, i.e., $\tau = \Lambda_1/U_1 \approx 0$. In this instance the analysis converges to a solution at S3 very close to that behind a normal shock, with uniform axial velocity and no change in the core radius or swirl. Gradual increase of τ leads to a solution at S3 with wakelike streamwise velocity, an expanded vortex core, and reduced swirl magnitude. For a typical case with $\gamma = 1.4$, $M_1 = 2.0$, and $U_1 = 600$ m/s, these trends continue until the axial velocity at the vortex axis stagnates when $\tau = 0.238$ and the system of equations does not converge for larger values of τ. This method has been used to obtain the vortex breakdown limit for a range of vortex strengths and freestream Mach numbers, the results of which have been used to generate a breakdown limit curve for NSVI. Note that the dependence of the shock strength on M_1 dictates that the breakdown limit for all uniform axial velocity supersonic vortices fall on a single curve of τ vs M_1.

Figure 4 shows the NSVI breakdown limit curve predicted using the current analysis. As can be seen from Fig. 4, an inverse relationship between the freestream Mach number and swirl ratio is predicted at breakdown, i.e., as M_1 increases the pressure ratio across the normal shock intensifies and the swirl ratio needed to cause breakdown is reduced. This breakdown limit curve can be directly compared with the NSVI experiments and inviscid numerical simulations involving uniform velocity vortices reported by Delery et al.,[5] which have been included in Fig. 4. At Mach numbers less than 2 the current analysis shows good correlation with both the experimental and numerical simulation breakdown limits. Above Mach 2, the current breakdown prediction is slightly higher than that reported by Delery et al.[5] but does exhibit the same leveling off of the swirl ratio required for breakdown as M_1 increases. In general the results of the current analytical method show good correlation with NSVI breakdown limits established by existing experimental data and numerical simulation.[5]

Results of the NSVI experiments reported in Ref. 7 are plotted with respect to the current breakdown limit in Fig. 5. In contrast to Ref. 5, these data do not correspond to points on the breakdown limit but to experiments involving particular vortex/shock combinations that were observed to either lead to vortex breakdown or not. Because the injector generated vortices involved in these experiments were observed to have a wakelike axial Mach number, the freestream velocity was not an appropriate parameter to be used for calculating the characteristic swirl ratio of the vortices. As an alternative, $\tau = (M_{sw}/M_{ax})_{max}$ was used as an approximate characteristic swirl ratio applicable to the nonuniform axial velocity vortices. When the swirl ratio is calculated in this manner, the current breakdown limit curve correctly predicts the presence of vortex breakdown in all but one of the NSVI experiments.[7]

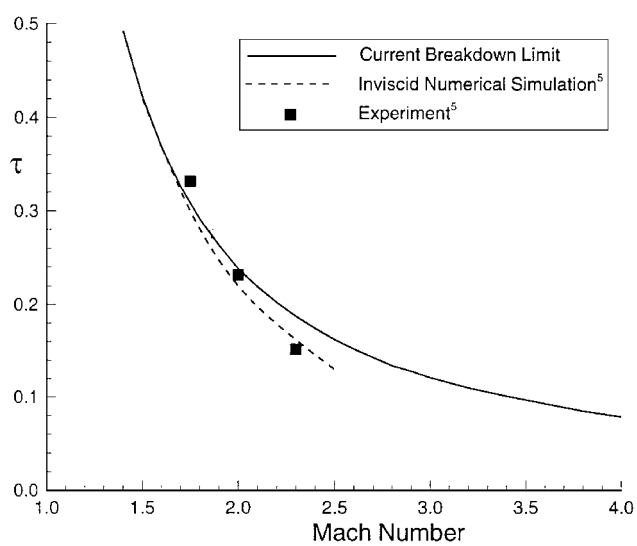

Fig. 4 Breakdown limit curve for NSVI in air.

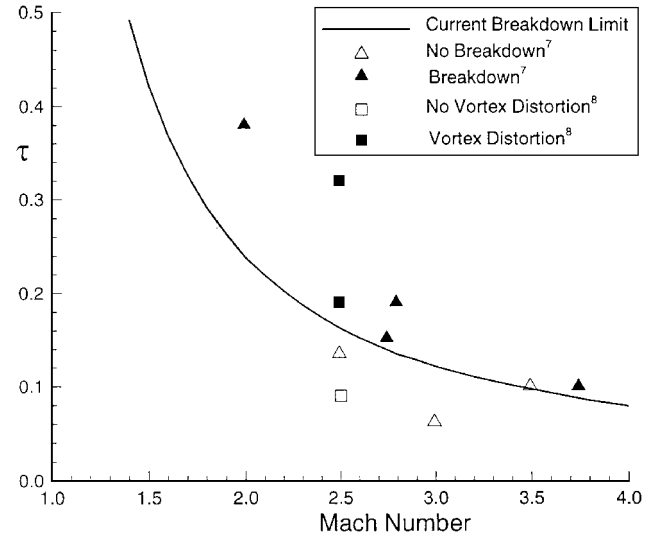

Fig. 5 Comparision of the NSVI breakdown limit curve with experimental data from Refs. 7 and 8.

The accuracy with which the current analysis reproduces the established NSVI breakdown limit curve[5] and correctly predicts breakdown in a number of NSVI experiments[7] is encouraging, particularly given the relative simplicity of the flow model. This suggests that, after the abrupt pressure rise imposed by a normal shock, a streamwise vortex does, in fact, attempt to return to a fully developed form, and the inability to do this leads to vortex breakdown. Modeling vortex breakdown as a dynamic phenomenon similar to boundary layer separation, therefore, appears to be a valid approach for NSVI. The accuracy of the current results also indicates that full numerical simulation is not needed to predict the onset of vortex breakdown in NSVI. The numerical breakdown limit of Ref. 5 was developed by performing a large number of numerical simulations over a range of vortex/shock combinations, requiring significant computational resources. As well as supplying insight into the physical mechanisms that lead to vortex breakdown in NSVI, the current analysis supplies a comparable breakdown limit to that reported in Ref. 5 while requiring orders of magnitude less computational resources.

A Rankine vortex with constant total enthalpy was used as a vortex model in the current work. However, the flow model can be applied to more realistic vortex models that include nonuniform axial velocity, nonuniform total enthalpy, and Burgers' vortex swirl distributions. Extension of the analysis to include these characteristics simply requires that all integrations used to determine pressure distributions, mass flows, and angular momentum flows be performed numerically. The current flow model, therefore, can be used to obtain theoretical estimates of postshock vortex properties and breakdown limits for NSVI involving a wide variety of vortex types.

NSVI Experiments

A series of NSVI experiments were performed in conjunction with the current analysis, the full results of which are reported in Kalkhoran et al.[8] The experimental configuration involved positioning an unswept rectangular half-wing upstream of a choked pitot type air intake in a Mach 2.5 flow. In the experiments, the supersonic wing tip vortex generated by the half-wing at angle of attack encountered the normal shock wave standing in front of the intake. Shadowgraph images taken during the experiments are interpreted here in light of the current predictions of NSVI induced vortex breakdown.

Measurements of the supersonic wing tip vortices generated by the half-wing at $\alpha = 5.7$ and 10.4 deg were reported in Ref. 16. These measurements showed that the wing tip vortices have a slightly asymmetric Burger-like swirl distribution in combination with a wakelike axial Mach number. As noted, a breakdown limit curve particular to each wing tip vortex could be developed using the observed wakelike axial Mach number distributions. However, for ease of comparison, breakdown predictions in the current work are performed using the breakdown limit curve of Fig. 4 and the approximate characteristic swirl ratio introduced in Ref. 7; i.e., $\tau = (M_{sw}/M_{ax})_{max}$. In other words, the behavior of the wing tip vortices in the presence of imposed normal shock waves is assumed to be similar to a vortex with uniform axial velocity and a swirl ratio equal to the maximum that occurs in the wing tip vortex. Maximum swirl ratios of $\tau_{5.7} = 0.18$ and $\tau_{10.4} = 0.32$ characterize the measured properties of the $\alpha = 5.7$ and 10.4 deg vortices, respectively. An image of the NSVI involving the vortex generated by the half-wing at $\alpha = 2.5$ deg is also presented. Unfortunately, a full survey of this vortex has not been conducted, so that the characteristic swirl ratio for this vortex is interpolated using a parabolic equation that passes through the higher angle-of-attack values and the origin ($\alpha = 0$ deg, $\tau = 0.0$), giving $\tau_{2.5} = 0.08$.

Instantaneous shadowgraph images of the undisturbed choked inlet and the NSVI involving the $\alpha = 2.5$, 5.7, and 10.4 deg vortices are shown in Figs. 6a–6d. Flow is from left to right in the images, and the stronger wing tip vortices in Figs. 6c and 6d can be seen to convect downstream from the wing toward the intake. It is clear even from a casual comparison of the images that the NSVI structure is strongly dependent on the vortex strength. Figure 6a shows a shadowgraph image of the flowfield with no half-wing, indicating that the undisturbed shock wave standing in front of the choked intake is smooth and normal to the freestream. Figure 6b shows an instantaneous image of the flowfield generated by the NSVI involving the $\alpha = 2.5$ deg vortex. The addition of the vortex can be seen to produce an upstream bulging of the shock wave, which was observed to exhibit some small-amplitude unsteadiness. Based on a comparison of Figs. 6a and 6b, it is clear that the flowfield reorganization characteristic of vortex breakdown is not induced by the introduction of the $\alpha = 2.5$ deg vortex.

The instantaneous shadowgraph images of the interactions involving the $\alpha = 5.7$ and 10.4 deg vortices shown in Figs. 6c and 6d indicate a dramatically different flow structure from Fig. 6b. In these instances, introduction of the vortices produces a significant upstream movement of the shock wave, which in turn generates a conical expansion of the vortex core well upstream of the intake. The images show a very interesting two-zone structure, described in Ref. 9 to be a subsonic internal flow containing the vortex core, surrounded by a supersonic outer flow. Both these NSVI flowfields were observed to undergo large-amplitude fluctuations, with the position of the conical apex oscillating between 30 and 80 mm upstream of the intake. The instantaneous images shown in Figs. 6c and 6d are typical for the respective flows and indicate that whereas the incoming vortex strengths are significantly different, the structure of both NSVI are quite similar. Some features commonly associated with incompressible vortex breakdown can be clearly seen when comparing Figs. 6c and 6d to the undisturbed flow in Fig. 6a, particularly the drastic reorganization of the flow and expansion of the vortex core. Definitive proof of the presence of a stagnation point and/or a recirculation region, however, was not reported in Ref. 8 due to the extreme difficulty of these measurements. The term vortex distortion was used in Ref. 9 to describe the observed structure.

Data points representing these NSVI experiments are included in Fig. 5. The point corresponding to the interaction involving the $\alpha = 2.5$ deg vortex falls below the breakdown limit curve. The current analysis, therefore, predicts no vortex breakdown for this interaction, a result consistent with the smooth, slightly distorted shock wave shown in Fig. 6b. The points corresponding to the interactions involving the $\alpha = 5.7$ and 10.4 deg vortices are above the breakdown limit curve; hence, vortex breakdown is predicted for these interactions. There would appear to be some correlation between the presence of vortex distortion in Figs. 6c and 6d and the prediction of vortex breakdown by the analysis. Given the accuracy of the current breakdown limit curve, and in light of recent measurements of supersonic vortex breakdown during vortex/cylinder interactions,[17] this correlation may be interpreted as circumstantial evidence that vortex distortion is, in fact, a form of vortex breakdown.

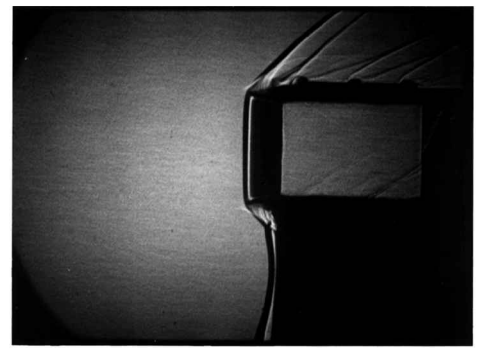

a) Choked inlet with no vortex

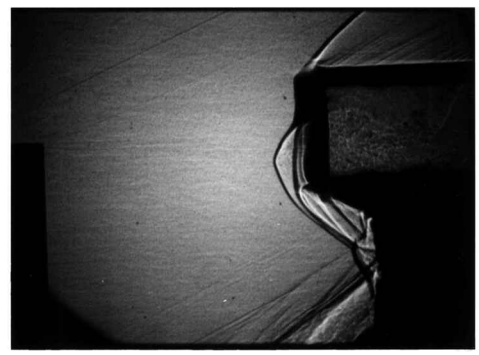

b) NSVI involving the $\alpha = 2.5$ deg wing tip vortex

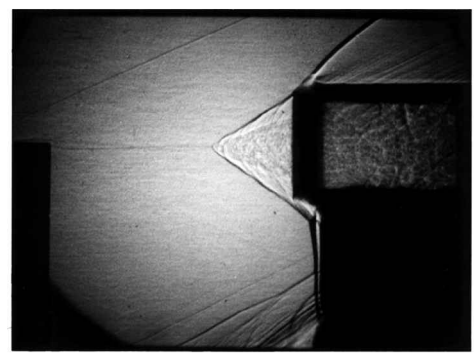

c) NSVI involving the $\alpha = 5.7$ deg wing tip vortex

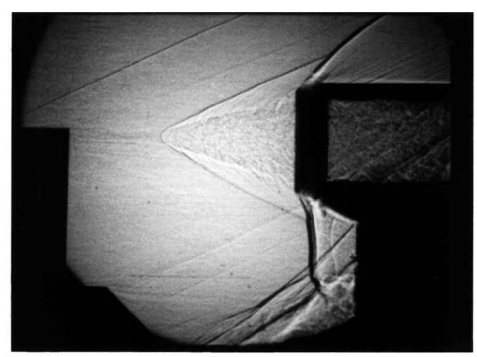

d) NSVI involving the $\alpha = 10.4$ deg wing tip vortex

Fig. 6 Shadowgraph images of the NSVI experiments.

Conclusions

An inviscid analysis designed to predict the onset of breakdown in NSVI has been presented. The analysis is based on a simplified model of the interaction, in which the rotational core of the vortex is treated as a slender swirling layer and a number of approximations

familiar from integral boundary layer methods are utilized. Vortex breakdown is presumed to occur when the perturbed vortex is not able to return to its fully developed form downstream of the shock without flow stagnation in its core region. This analysis supplies a breakdown limit curve indicating an inverse relationship between vortex swirl and freestream Mach number at breakdown. Comparison of this breakdown limit with established experimental data and results of inviscid numerical simulations showed that the analytical method accurately predicts vortex breakdown over a wide Mach number range. The good correlation between established breakdown limits and this analysis suggests that the current model contains the dominant physical mechanisms that lead to normal shock wave induced vortex breakdown and that numerical simulation is not required to predict the onset of vortex breakdown in these flows. Vortex breakdown predictions were also found to correspond with the presence of vortex distortion in a number of NSVI experiments. This fact was interpreted as circumstantial evidence that vortex distortion is a form of vortex breakdown.

References

[1]Lambourne, N. C., and Bryer, D. W., "The Bursting of Leading-Edge Vortices—Some Observations and Discussion of the Phenomenon," Aeronautical Research Council, Rept. 3282, London, April 1961.

[2]Harvey, J. K., "Some Observations of Vortex Breakdown Phenomenon," *Journal of Fluid Mechanics*, Vol. 14, 1962, pp. 585–592.

[3]Faler, J. H., and Leibovich, S., "An Experimental Map of the Internal Structure of a Vortex Breakdown," *Journal of Fluid Mechanics*, Vol. 86, Pt. 2, 1978, pp. 313–335.

[4]Sarpkaya, T., "On Stationary and Traveling Vortex Breakdowns," *Journal of Fluid Mechanics*, Vol. 45, Pt. 3, 1971, p. 585.

[5]Delery, J., Horowitz, E., Leucther, O., and Solignac, J. L., "Fundamental Studies on Vortex Flows," *La Recherche Aerospatiale*, English ed., No. 2, 1984, pp. 81–104.

[6]Metwally, O., Settles, G. S., and Hortsman, C., "An Experimental Study of Shock Wave/Vortex Interaction," AIAA Paper 89-0082, Jan. 1989.

[7]Cattafesta, L. N., and Settles, G. S., "Experiments on Shock/Vortex Interaction," AIAA Paper 92-0315, Jan. 1992.

[8]Kalkhoran, I. M., Smart, M. K., and Betti, A., "Interaction of a Supersonic Wing Tip Vortex with a Normal Shock," *AIAA Journal*, Vol. 34, No. 9, 1996, pp. 1855–1861.

[9]Kalkhoran, I. M., "Vortex Distortion During Vortex-Surface Interaction in a Mach 3 Stream," *AIAA Journal*, Vol. 32, No.1, 1994, pp. 123–129.

[10]Erlebacher, G., Hussaini, M. Y., and Shu, C. W., "Interaction of a Shock with a Longitudinal Vortex," NASA CR-198332, Inst. for Computer Applications in Science and Engineering, ICASE Rept. No. 96-31, 1996.

[11]Hall, M. G., "Vortex Breakdown," *Annual Review of Fluid Mechanics*, Vol. 4, 1972, pp. 195–218.

[12]Leibovich, S., "Vortex Stability and Breakdown: Survey and Extension," *AIAA Journal*, Vol. 22, No. 9, 1983, pp. 1192–1206.

[13]Delery, J. M., "Aspects of Vortex Breakdown," *Progress in Aerospace Sciences*, Vol. 30, No. 1, 1994, pp. 1–59.

[14]Stewartson, K., and Hall, M. G., "The Inner Solution for the Core of a Leading Edge Vortex," *Journal of Fluid Mechanics*, Vol. 15, 1963, pp. 306–318.

[15]Batchelor, G. K., "Axial Flow in Trailing Line Vortices," *Journal of Fluid Mechanics*, Vol. 20, 1964, pp. 645–658.

[16]Smart, M. K., Kalkhoran, I. M., and Bentson, J., "Measurements of Supersonic Wing Tip Vortices," *AIAA Journal*, Vol. 33, No. 10, 1995, pp. 1761–1768.

[17]Kalkhoran, I. M., Wang, F. Y., Milanovic, I., and Smart, M. K., "Supersonic Vortex Breakdown During Vortex/Cylinder Interaction," ASME Fluids Engineering Div. Summer Meeting, American Society of Mechanical Engineers, Paper FEDSM97-3319, June 1997.

W. Oberkampf
Associate Editor